ELSEVIER

Heterostructures based on two-dimensional layered materials and their potential applications

Ming-Yang Li[1,2], Chang-Hsiao Chen[2], Yumeng Shi[1] and Lain-Jong Li[1,*]

[1] Physical Sciences and Engineering Division, King Abdullah University of Science and Technology, Thuwal 23955-6900, Saudi Arabia
[2] Institute of Atomic and Molecular Sciences, Academia Sinica, Taipei 10617, Taiwan

The development of two-dimensional (2D) layered materials is driven by fundamental interest and their potential applications. Atomically thin 2D materials provide a wide range of basic building blocks with unique electrical, optical, and thermal properties which do not exist in their bulk counterparts. The van der Waals interlayer interaction enables the possibility to exfoliate and reassemble different 2D materials into arbitrarily and vertically stacked heterostructures. Recently developed vapor phase growth of 2D materials further paves the way of directly synthesizing vertical and lateral heterojunctions. This review provides insights into the layered 2D heterostructures, with a concise introduction to preparative approaches for 2D materials and heterostructures. These unique 2D heterostructures have abundant implications for many potential applications.

Introduction

The heterostructures formed by alien semiconductors play an important role in modern semiconductor industry, and they have been widely used as an essential building block for electronic devices. A heterojunction can be formed by interfacing two different semiconductors, where the electronic band structure near the interface will be changed according to electrostatics. The semiconductor heterojunctions have been applied in many solid-state devices, such as solar cells, photo detectors, semiconductor lasers, and light-emitting diodes (LEDs). Since the great influence of the semiconductor junction to our daily life, Nobel Prize in physics was awarded to Zhores I. Alferov, Herbert Kroemer and Jack S. Kilby for their contribution toward the development of semiconductor heterostructures [1,2] and to Isamu Akasaki, Hiroshi Amano, and Shuji Nakamura for the invention of blue LEDs [3,4].

Two-dimensional (2D) materials commonly possess unique optical bandgap structures, extremely strong light–matter interactions, and large specific surface area. Graphene, hexagonal boron nitride (h-BN) and some transition metal dichalcogenides (TMDs) have emerged as promising building blocks for novel nanoelectronics, providing a full range of materials types, including large band gap insulators [5,6], semiconductors [7,8], and semimetals [9,10]. 2D semiconductors exhibit high carrier mobility, high on-off current ratio and excellent bendability that suit for future low-power consumption and flexible electronics [11–15]. These materials are laterally composed by strong covalent bonds, which provide great in-plane stability. On the other hand, the weak van der Waals (vdW) interlayer force allows us to isolate 2D monolayer and restack them into arbitrary stacking heterojunctions without the need to consider the atomic commensurability as in their bulk counterparts. Hence, a new research field of heterojunctions formed by 2D layered materials has emerged [16–18]. The vertically stacked 2D layers can be formed by mechanical stacking, serving as a quick and convenient way of forming heterostructures. Besides, the chemical vapor deposition (CVD) method is a growing category for fabricating 2D heterojunction in the past few years. CVD process not only provides large-area 2D material for mechanical assembling. It is also possible to grow various stacking structures directly. The synthesized heterojunction can provide a much cleaner interface for fundamental research and hence better device performance. Furthermore, the development of this methodology has shown the possibility to synthesize lateral 2D heterojunction, which goes beyond the limit of the mechanical stacking method. 2D lateral

*Corresponding author:. Li, L.-J. (lance.li@kaust.edu.sa)

 http://dx.doi.org/10.1016/j.mattod.2015.11.003

heterojunction has opened a new realm in material science and device applications. This review focuses on the preparation and applications of the heterostructures from various 2D layered materials.

Preparation of 2D materials

The first successful method to obtain 2D materials is through the mechanical exfoliation of their bulk crystals using scotch tapes (Fig. 1a) [19,20]. With this method, monolayer or few-layer flakes can be obtained without introducing too many defects. Although this method is not suitable for large-scale production, the mechanically exfoliated films normally exhibit high crystallinity compared with the samples obtained via other approaches. To further enhance the production of 2D materials, the chemical exfoliation methods such as electrochemical exfoliation [21,22], solvents assistance exfoliation [23] and lithium intercalation approaches (Fig. 1b) [24–28] have been developed. These approaches can provide massive 2D nanoflakes in solutions but the lateral size and thickness of the flakes cannot be precisely controlled. The quality of the 2D flakes usually degrades under chemical process, which remains as an issue in this field.

In addition to the exfoliation method, vaporized precursors can react to form monolayer 2D materials in a CVD chamber at an elevated temperature and this method shows the capability for wafer-scale synthesis, which is desirable for practical production. Various 2D materials have been successfully synthesized by CVD approaches including graphene on copper [9,29], and TMDs monolayers (such as MoS_2 [30–32], WS_2 [33,34], WSe_2 [14] and $MoSe_2$ [35,36]) on sapphire substrates. Here we take MoS_2 synthesis as the example to discuss the progress of CVD methods. In 2012, Liu and co-workers have reported a two-step thermolysis process as shown in Fig. 1c [8], where a three-layered MoS_2 sheets can be achieved. To improve the crystallinity, Lee and co-workers demonstrate a direct CVD synthesis using MoO_3 and S as the sources (Fig. 1d) [32]. During the growth, MoO_3 is heated into vapor phases and reacted with S vapors followed by a two-step reaction, which allows the growth of monolayer and single-crystalline MoS_2 flakes on desired substrates. Furthermore, Lin and co-workers have shown that wafer-scale deposition can be achieved by using the same chemistry [37], where the few-layer MoS_2 was obtained after direct sulfurization of MoO_3 thin-films on sapphire substrates. Due to its simplicity and reproducibility, direct sulfurization or selenization of various metal oxides have been widely adopted to produce TMDs layer such as MoS_2 [38], WS_2 [39,40], $MoSe_2$ [35].

Fabrication of 2D heterostructures

Owing to the layer structures of 2D materials, the formation of heterostructure can be in vertical or lateral fashion. Depending on the architecture of the heterostructures, the fabrication methods vary. Here, we sort the fabrication processes into two categories: one is the mechanical stacking method and the other is the directly synthesis.

Heterostructures by manual stacking

Thanks to the invention of exfoliation [19] and transfer [41,42] methods of layered materials, the mechanically or chemically exfoliated 2D flakes can be manually stacked to form 2D heterostructures, where the interlayer vdW force holds the heterostructure securely. The 2D flakes can be mechanically/chemically exfoliated from bulk materials or isolated from the synthetic (grown) 2D layers on substrates. The stacking order and the interface of the heterojunction are critical for their electrical and optical properties. The possibility to form various stacking lattice orientation provides the heterojunction interface with

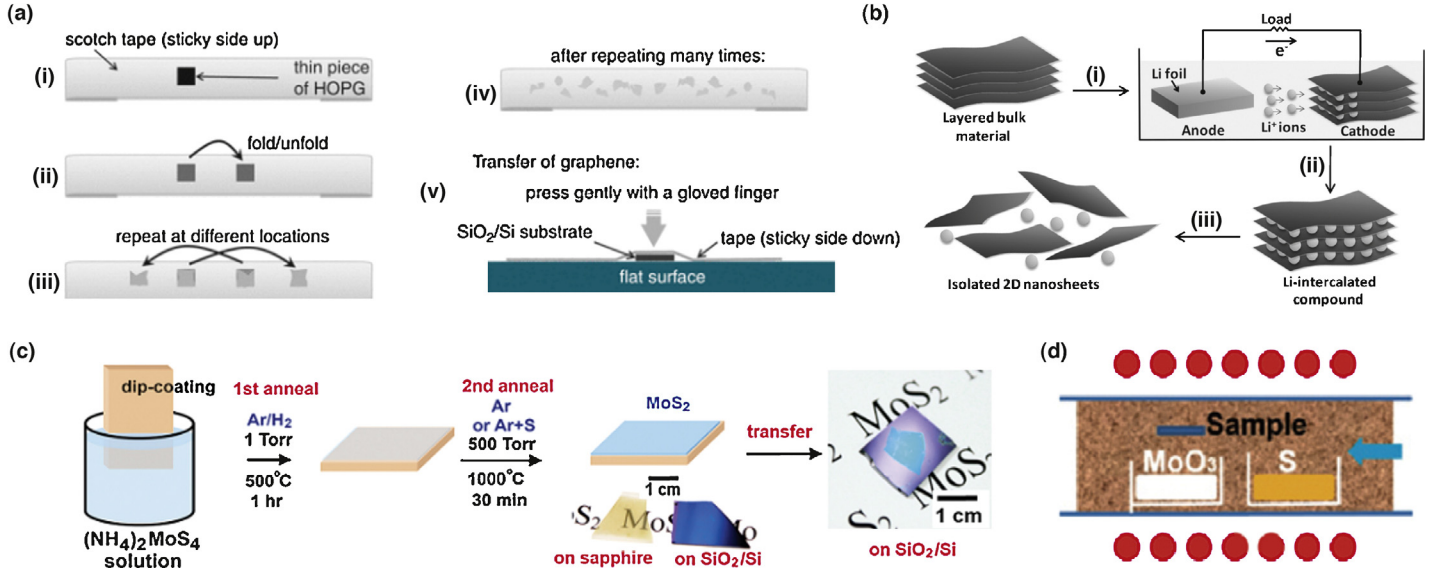

FIGURE 1

Schematic illustration of mechanical and chemical exfoliation processes and synthetic methods for 2D material production. (a) Steps of the mechanical exfoliation process for 2D material isolation [20]. Reproduced with permission from Ref [20]. Copyright 2012, Springer Science + Business Media B.V. (b) Steps of the electrochemical lithiation and intercalation process for 2D nanosheet production [27]. Reproduced with permission from Ref [27]. Copyright 2011 WILEY-VCH Verlag GmbH & Co. KGaA, Weinheim (c) The two-step thermolysis process for few-layer MoS_2 growth [8]. Reproduced with permission from Ref [8]. Copyright 2012, American Chemical Society. (d) The experimental set-up for MoS_2 synthesis through the gas phase reaction of MoO_3 and S [32]. Reproduced with permission from Ref [32]. Copyright 2011 WILEY-VCH Verlag GmbH & Co. KGaA, Weinheim.

tunable physical properties depending on the interaction strength of the two layered materials. For example, the carrier mobility of graphene on SiO_2 is normally limited by the scattering effect from charge impurities, substrate surface roughness and SiO_2 optical phonons. Dean and co-workers have demonstrated a graphene device on h-BN interface layers by using mechanical tacking method (Fig. 2a) [42]. The atomic flat and nearly free charge trapping of h-BN layers serves as excellent substrate for graphene. The carrier mobility of graphene devices fabricated on h-BN substrates is nearly an order higher than the devices on amorphous SiO_2 substrates. The graphene layers on h-BN show reduced roughness, less doping and improved chemical stability, demonstrating the critical role of the interfaces. On the other hand, Hsu and co-workers perform the second harmonic generation (SHG) measurement to

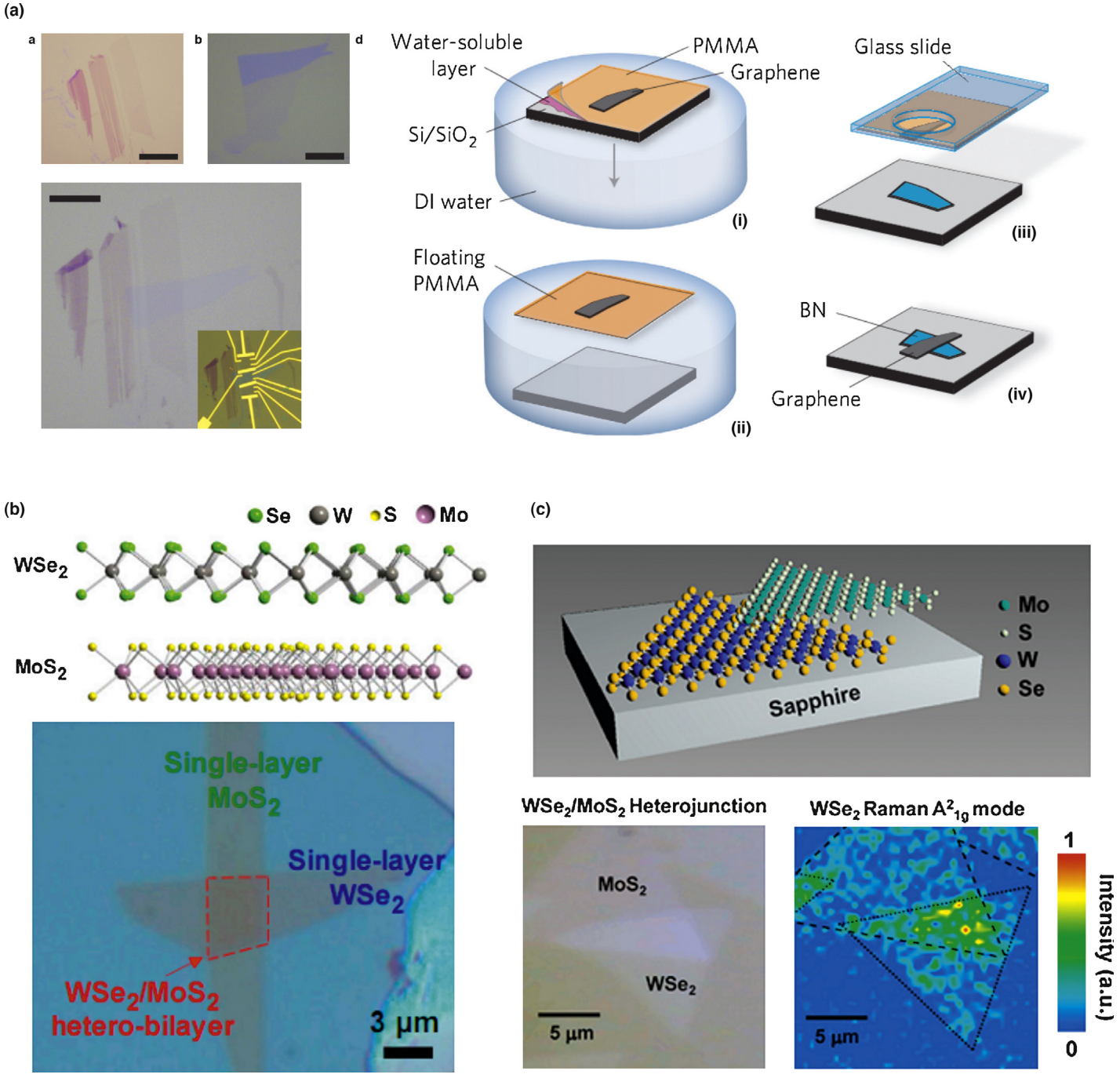

FIGURE 2

Mechanical stacking process for vertical heterostructures. (a) Schematic illustration of the transfer and stacking process and the optical image of the graphene/h-BN devices (scale bars, 10 μm) [42]. Reproduced with permission from Ref [42]. Copyright 2010, Nature Publishing Group. (b) Schematic illustration and optical microscope image of the stacked WSe_2/MoS_2 heterojunction [44]. Reproduced with permission from Ref [44]. Copyright 2014, National Academy of Sciences. (c) Schematic illustration and optical microscope image of the CVD MoS_2/WSe_2 stacking heterojunction. The spatial mapping of the Raman intensity for WSe_2 A^2_{1g} peak shows the interlayer coupled area [45]. Reproduced with permission from Ref [45]. Copyright 2014, American Chemical Society.

demonstrate the effect of the twisting angle on stacking TMD bilayers [43]. The SHG from the twisted bilayers is a coherent superposition of the second harmonic fields from the individual stacking layers and the phase difference is only determined by the stacking angle. For the interlayer coupling, Fang and co-workers have investigated the optical transition properties on MoS_2/WSe_2 stacking heterojunction (Fig. 2b) [44]. The band alignment and the interlayer coupling at the interface result in a Stokes shift of ~100 meV, where the direct absorption and indirect emission were observed on the heterojunction. Chiu and co-workers have fabricated vertical MoS_2/WSe_2 heterojunction by manually stacking CVD-grown MoS_2 and WSe_2 monolayers and demonstrated that the interlayer coupling can be enhanced by thermal treatment (Fig. 2c) [45]. Through the study on interlayer coupling with optical transition and the band alignment with scanning tunneling spectroscopy (STS) and X-ray photoemission spectroscopy (XPS), the band alignment and the exciton binding energy of the heterojunction can be determined. The mechanical stacking method provides a simplest way to construct arbitrary 2D heterostructures. However, the quality of the interface can be easily affected by the trapping of solvents or chemicals used for transfer, which still remains as an issue to be solved.

Direct synthesis of 2D heterostructures:

Although the exfoliation technique can produce high quality 2D crystals for fundamental study, it still remains challenging to control the location, layer number and interface of the produced heterojunction, which hinders the practical fabrication. Very recently, the CVD technique shows great promise for the production of large domain 2D building blocks for TMD heterostructures. It also allows the direct synthesis of various 2D heterojunctions with vertically stacked or laterally stitched interface. Here, we introduce the vertical and lateral heterojunctions fabricated by CVD method separately.

Vertically stacked 2D heterojunctions

With the CVD methods, the vertically stacked heterojunction can be obtained by growing one 2D material on another. The direct growth in principle results in clean heterojunction interfaces. Since there exists only vdW interaction between 2D layers, the mechanism is likely through the vdW epitaxy, where the lattice mismatch is the key challenge to overcome. The early experiment starts from graphene and h-BN which share similar lattice constant. Yang and co-workers have reported a plasma-assisted deposition method for the growth of single domain graphene on h-BN substrate (Fig. 3a) [46]. Graphene registers on the h-BN lattice with a preferred orientation and the size of graphene is only restricted by the area of underlying h-BN. Furthermore, Shi and co-workers have obtained a vertically stacked MoS_2/graphene structure via thermal decomposition of ammonium thiomolybdate precursors on graphene surfaces (Fig. 3b) [47]. Note that although the lattice constant of MoS_2 is about 28% larger than that of graphene, graphene is still a good growth platform for MoS_2. It is likely that the vertical epitaxial growth can tolerate the crystal orientation difference and the growth of MoS_2 on graphene may involve strain to accommodate the lattice mismatch. Lin and co-workers have further demonstrated the direct growth of MoS_2, WSe_2, and h-BN on graphene through CVD methods, where the underlying

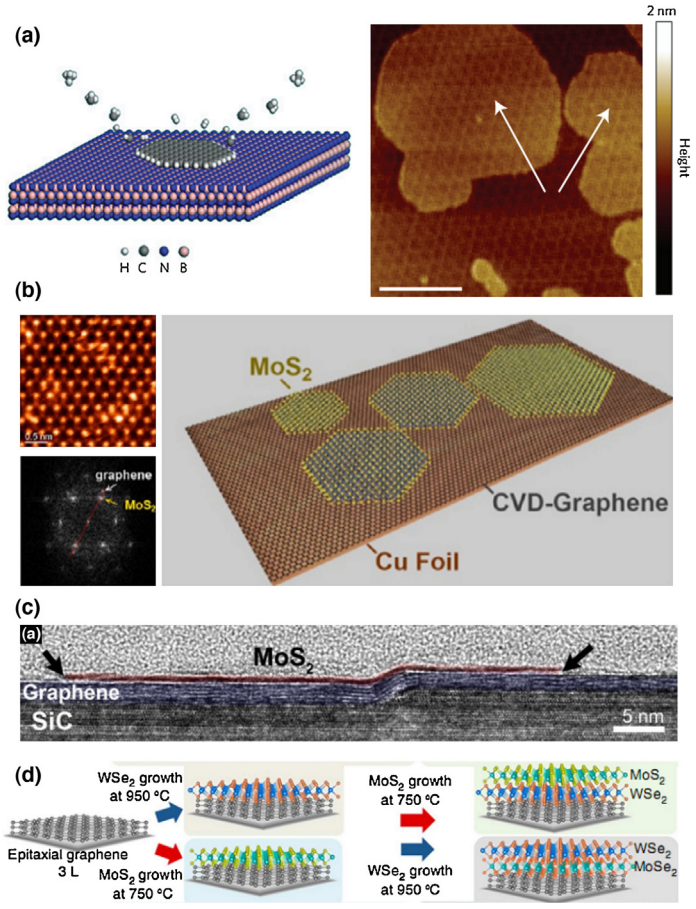

FIGURE 3

Growth of 2D vertical heterostructures. (a) Schematic illustration of the plasma-assisted deposition method for graphene grown on h-BN and the Morié pattern of the heterostructure. The white arrows indicate the graphene layer (scale bars 100 nm) [46]. Reproduced with permission from Ref [46]. Copyright 2013, Nature Publishing Group. (b) The TEM image and the schematic illustration of the MoS_2 grown on graphene [47]. Reproduced with permission from Ref [47]. Copyright 2012, American Chemical Society. (c) Cross-sectional HRTEM of MoS_2/graphene stacked heterojunction on a SiC substrate step edge [48]. Reproduced with permission from Ref [48] Copyright 2014, American Chemical Society. (d) Schematic illustration of the MoS_2/WSe_2/graphene and WSe_2/MoS_2/graphene vertical heterostructures formed by oxide powder vaporization and MOCVD approaches [50]. Reproduced with permission from Ref [50]. Copyright 2015, Nature Publishing Group.

graphene was grown epitaxially on SiC (Fig. 3c) [48]. It has been revealed that the morphology of the graphene layer strongly affects with the growth and the properties of top heterostructures, where strain, wrinkling, and defects on the surface of graphene provides the nucleation centers for upper layer material growth. Another research interest is focused on TMD heterojunctions formation. Gong and co-workers have reported a one-step vapor phase growth method for the direct formation of vertical WS_2/MoS_2 heterostructures [49]. The WS_2 can grow on top of MoS_2 with the 2H stacking structure. On the other hand, Lin and co-workers present the direct synthesis of MoS_2/WSe_2/graphene and WSe_2/MoS_2/graphene heterostructures *ex situ* by oxide powder vaporization and metal-organic chemical vapor deposition (MOCVD) methods as shown in Fig. 3d [50]. The electrical transport of the heterostructure exhibits a sharp negative

differential resistance at room temperature resulting from the special resonant tunneling of charge carriers at interface. This observation has not been found in mechanically stacked junctions. These direct syntheses are in principle applicable to other materials which opens new ways for the fabrication of various heterojunctions. However, the thermodynamically dominated process might restrict the controllability on stacking order, twisting angle or domain size.

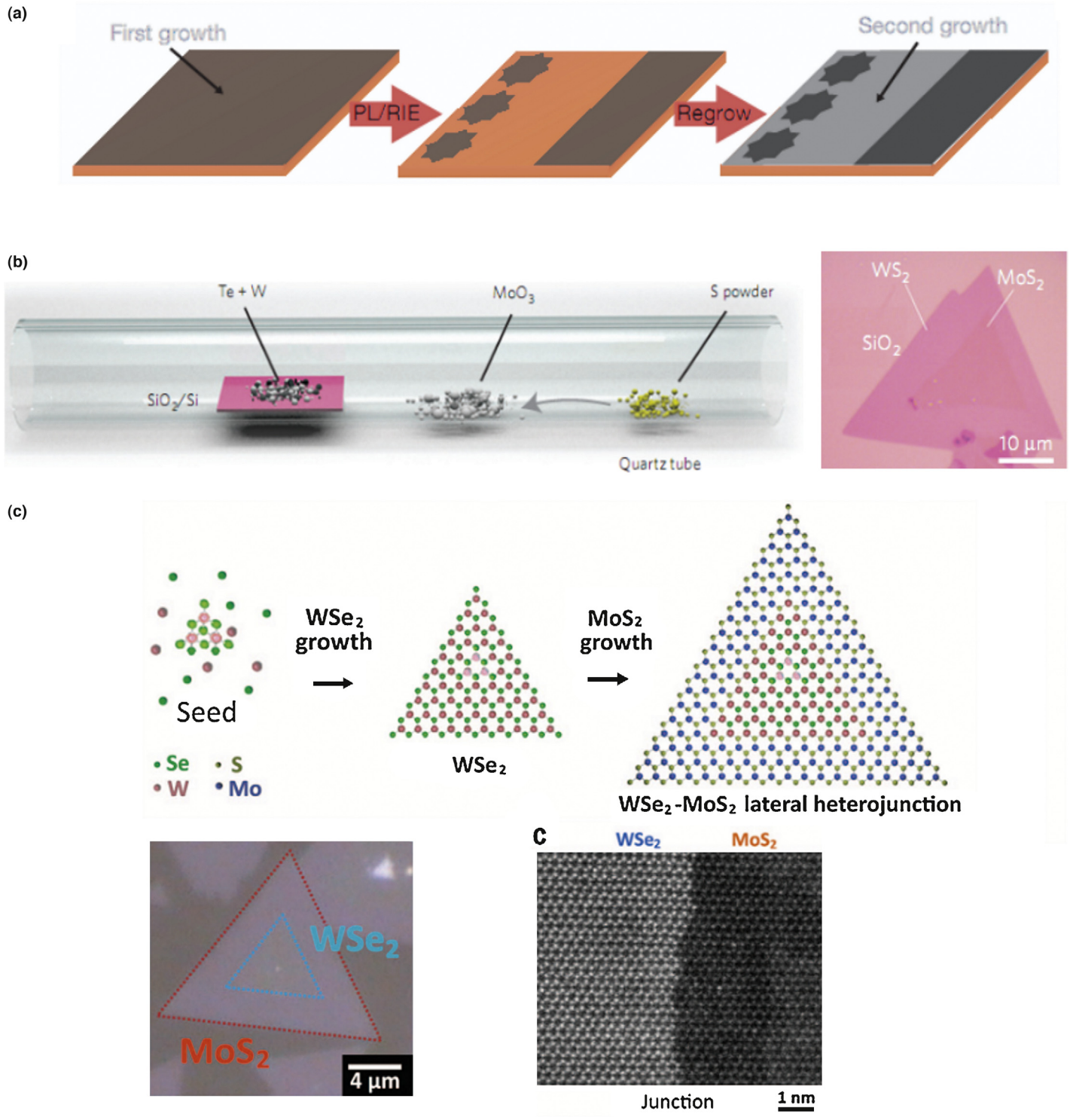

FIGURE 4

In-plane epitaxial growth of 2D lateral heterostructures. (a) Schematic illustration for formation of graphene/h-BN lateral heterojunctions using CVD growth method [51]. Reproduced with permission from Ref [51]. Copyright 2012, Nature Publishing Group. (b) Schematic illustration of the one-pot synthesis setup and optical image of the WS_2/MoS_2 lateral heterojunction [49]. Reproduced with permission from Ref [49]. Copyright 2014, Nature Publishing Group. (c) Schematic illustration of the two-step growth of the monolayer WSe_2/MoS_2 lateral heterojunction, and the optical image of the junction. The right picture shows the corresponding High-resolution STEM images taken at the interface [55]. Reproduced with permission from Ref [55]. Copyright 2015 American Association for the Advancement of Science.

TABLE 1

2D heterostructures and applications.

Heterojunction type	Layer structure	Application	Device performance	Ref
Semi-metal/ semiconductor	Graphene/MoS_2	DNA biosensor	Detection DNA concentration 1 atto mole	Loan et al. [60].
	Graphene/WS_2	Solar cells	Power conversion efficiency 3.3%	Shanmugam et al. [67]
	Graphene/WS_2/graphene/ h-BN	Vertical FETs	ON/OFF ratio $>1 \times 10^6$	Georgiou et al. [75]
	Graphene/MoS_2	Vertical FETs	Current density 5000 A cm^{-2} ON/OFF ratio $>10^3$	Yu et al. [76]
	Graphene/MoS_2	Vertical FETs	Current density $\sim 10^4$ A cm^{-2} ON/OFF ratio $\sim 10^5$	Moriya et al. [77]
	Graphene/h-BN/MoS_2/ graphene	FETs	Electron mobility $\sim$33 cm^2/V s. ON/OFF current ratio $>10^6$	Roy et al. [68]
	Graphene/MoS_2/graphene	Photodetector	External quantum efficiency 55% Internal quantum efficiency 85% Photoresponsivity 0.22 A/W	Yu et al. [80]
	Graphene/WS_2/graphene	Photodetector	External quantum efficiency $\sim$30% Photoresponsivity 0.1 A/W	Britenall et al. [79]
	Graphene/MoS_2	Photodetector	Photogain $>10^8$ Internal quantum efficiency $\sim$15% Photoresponsivity $>10^7$ A/W	Zhang et al. [89]
	Graphene/MoS_2	Photodetector	Gain $\sim$5–10 $\times 10^{10}$ Quantum efficiency $\sim$32% Photoresponsivity 1×10^{10} A/W at 130 K, 5×10^8 A/W at room temperature	Roy et al. [90]
	Graphene/h-BN/MoS_2(WS_2)/ h-BN/graphene	Electroluminescence	Extrinsic quantum efficiency $\sim$10%	Withers et al. [88]
Semi-metal/insulator	Graphene/h-BN	FETs	Mobility 60,000 cm^2/V s	Dean et al. [42]
	h-BN/Gra./h-BN/Gra./h-BN; h-BN/Gra./MoS_2/Gra./h-BN	Vertical FET	B/G/B/G/B: ON/OFF ratio 50 B/G/M/G/B: ON/OFF ratio 1×10^4	Britnell et al. [74]
	Graphene/h-BN/graphene	Thermoelectrical power	Seebeck coefficient $-$99.3 μV/K $ZT = 1.05 \times 10^{-6}$	Chen et al. [92]
Semiconductor/ semiconductor	WSe_2/MoS_2	Solar cells	Power conversion efficiency 0.2% External quantum efficiency 1.5%	Furchi et al. [63]
	p-WSe_2/n-WSe_2	CMOS	Full logic swing voltage gain up to 38	Yu et al. [76]
	p-MoS_2/n-MoS_2	Solar cells	Power conversion efficiency 2.8%	Wi et al. [65]
	MoS_2/p-Si	Solar cells	Power conversion efficiency 5.23%	Tsai et al. [66]
	WSe_2/MoS_2	Solar cells	Photoresponsivity is $\sim$2 mA W^{-1}	Lee et al. [64]
	Gra./WSe_2/MoS_2/Gra.		Photoresponsivity is $\sim$10 mA W^{-1} External quantum efficiency 2.4%, 12% and 34% for monolayer, bilayer and multi-layer TMDs	
	WSe_2/MoS_2	p–n diode Photodetector Electroluminescence	Current rectification factor 1.2 External quantum efficiency 12%	Cheng et al. [81]
	Black phosphorus/MoS_2	p–n diode Photodetector	Current rectification factor 10^5 External quantum efficiency 0.3% Photoresponsivity 418 mA/W	Deng et al. [82]
	MoS_2/WS_2	Charge transfer	Ultrafast hole transfer time $<$50 fs.	Hong et al. [93]
	WS_2/MoS_2	Solar cells	Open-loop voltage 0.12 V Close-loop current 5.7 pA	Gong et al. [49]
	WSe_2/WS_2	Solar cells	Open-loop voltage $\sim$0.47 V Close-loop current $\sim$1.2 nA	Duan et al. [53]
	WSe2/MoS2	Solar cells	Open-loop voltage $\sim$0.22 V Close-loop current $\sim$7.7 pA	Li et al. [55]
	WSe2/MoSe2	Solar cells	Power conversion efficiency 0.12%	Gong et al. [56]
	MoS_2/p-Ge	Band-to-band tunneling FET	Subthreshold swing minimum of 3.9 mV/decade, average 31.1 mV/decade	Sarkar et al. [78]
	MoS2/p-Si	Solar cells Electroluminescence	External quantum efficiency 4%	Lopez-Sanchez et al. [83]
Semiconductor/ insulator	MoS_2/h-BN/graphene	FETs	Mobility $>$45 cm^2/V s ON/OFF ratio 10^4–10^6	Lee et al. [94]

Laterally stitched 2D heterojunctions

Since the 2D materials are covalently bonded, the lateral heterojunction can only be formed by direct growth. Levendorf and co-workers have demonstrated the lateral stitched graphene/h-BN heterojunction by growing h-BN on patterned graphene with CVD method, which results in a continuous 2D heterojunction film (Fig. 4a) [51]. Note that the general issue for lateral heterojunction is the strain release between two materials. Lu and co-workers have used *in situ* scanning tunneling microscopy to study the interface of graphene/h-BN lateral junction on a Ru(0001) surface to understand how the lattice strain can be released along the lateral direction [52]. The defect-free, pseudomorphic growth of h-BN from graphene edge occurs only within a short distance (<1.29 nm) perpendicular to the interface and the zero-dimensional dislocations occur to release the elastic strain energy and to stabilize the structure. For the lateral TMD heterojunction, the early demonstration has been achieved by one-pot synthesis. For example, the $MoS_2/MoSe_2$ and WS_2/WSe_2 lateral heterojunctions are obtained by physical vapor transport method with sequential source switching [53], $MoSe_2/WSe_2$ by physical vapor transport method with mixed sources [54] and WS_2/MoS_2 by one-spot CVD growth with multi-sources (Fig. 4b) [49]. Atomically resolved tunneling electron

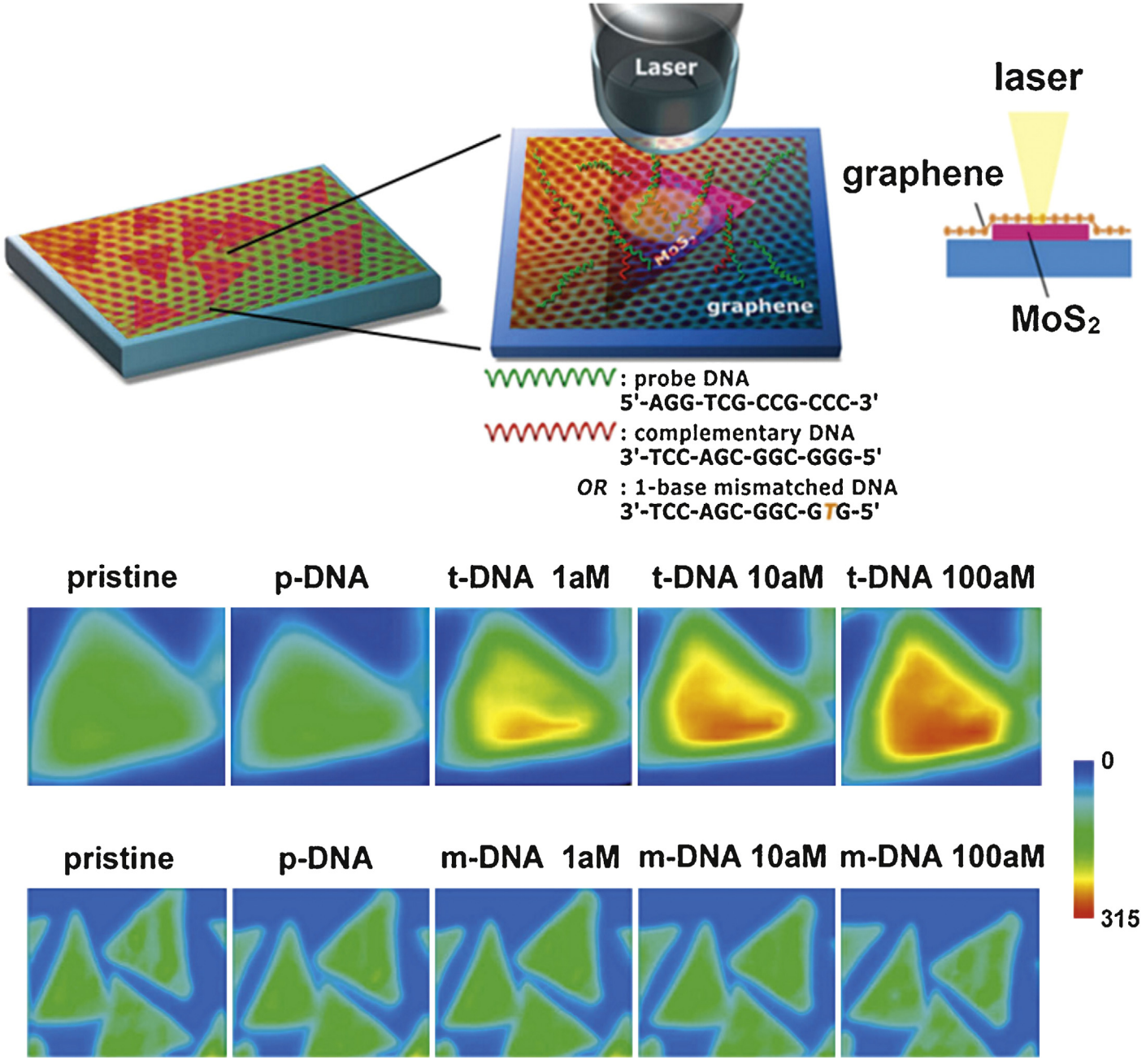

FIGURE 5

Heterostructures for biosensor. Schematic illustration of the graphene/MoS_2 stacking heterostructure sensor and measurement setup [60]. Bottom images show the MoS_2 photoluminescence peak mappings when hybridized with the complementary target DNA (up) and the mismatched DNA (down) at different concentrations. Reproduced with permission from Ref [60]. Copyright 2014, WILEY-VCH Verlag GmbH & Co. KGaA, Weinheim.

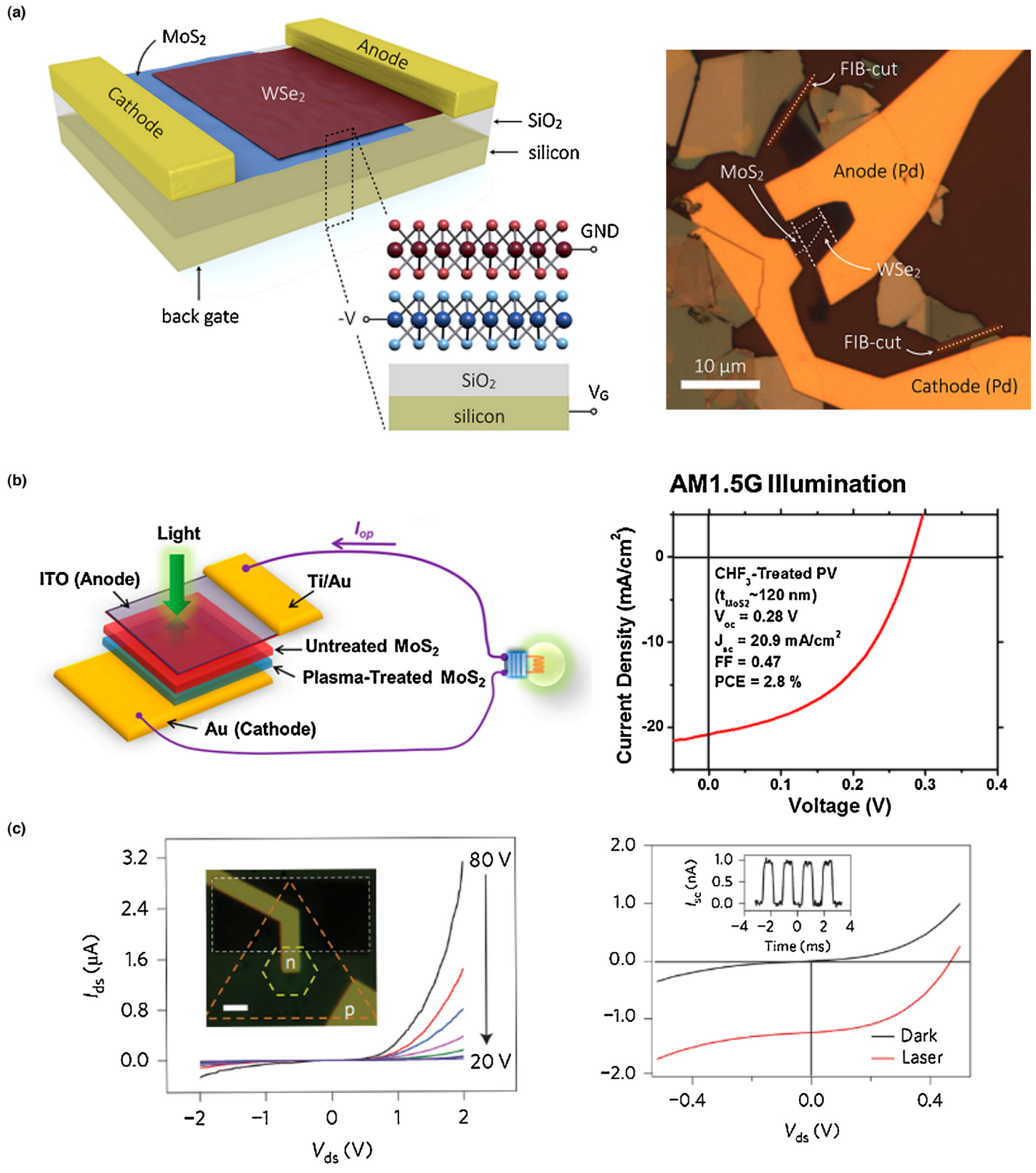

FIGURE 6

Heterostructures for photovoltaic devices. (a) Schematic illustration and optical microscope image of the MoS_2/WSe_2 hetero-diode [63]. (b) Schematic illustration of the p-MoS_2/n-MoS_2 photovoltaic device and the current-voltage characteristics under AM1.5 G solar simulator illumination [65]. Reproduced with permission from Refs [63,65]. Copyright 2014, American Chemical Society. (c) The optical image of the lateral WSe_2/WS_2 heterojunction p–n diode and its *I–V* characterization under different gate voltage (left) and under laser illumination (right). Scale bar, 2 μm [53]. Reproduced with permission from Ref [53]. Copyright 2014, Nature Publishing Group.

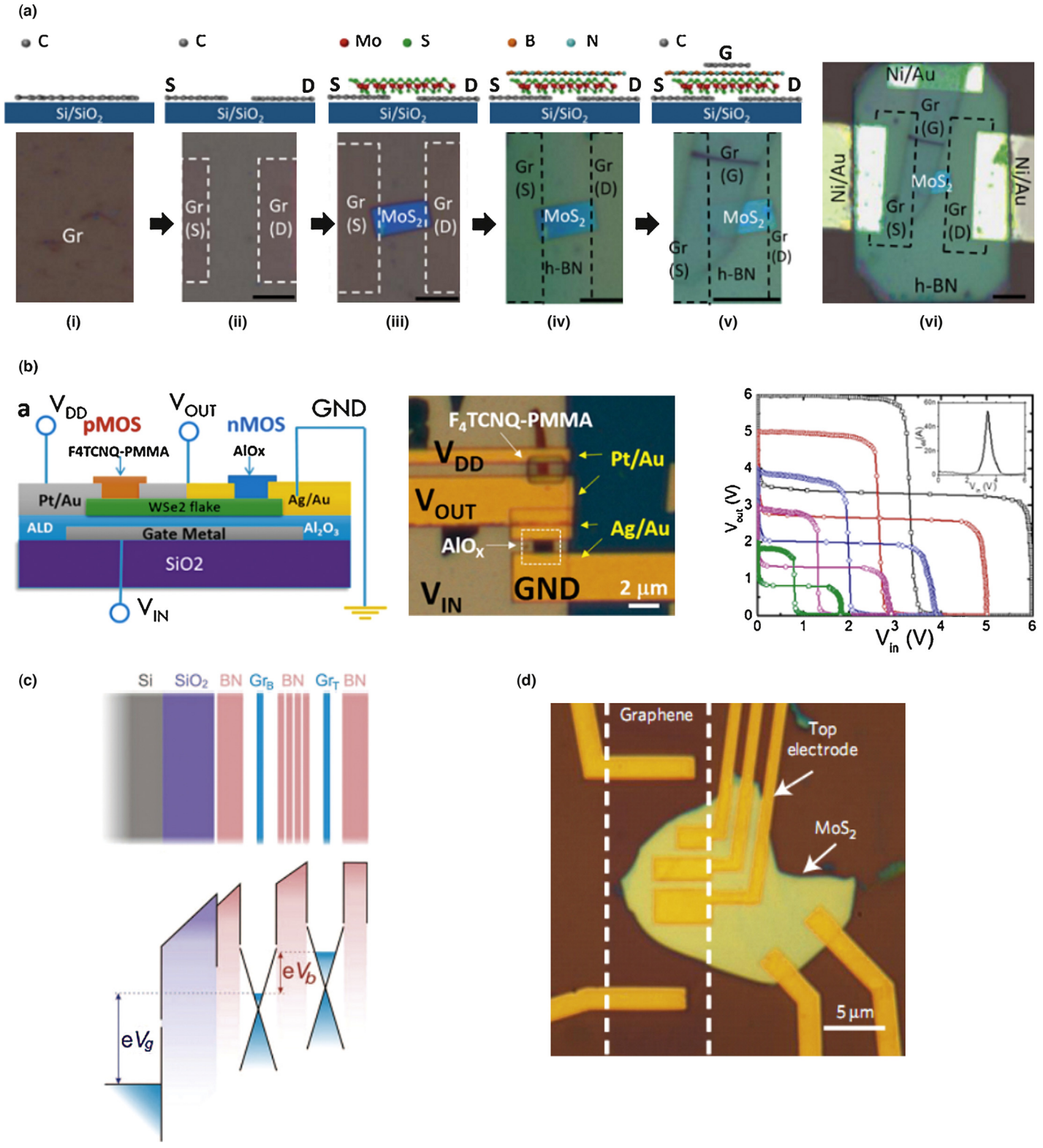

FIGURE 7

Heterostructures for field-effect transistors. (a) Schematic illustration of the fabrication process and the related optical images of the all-2D FETs [68]. Reproduced with permission from Ref [68]. Copyright 2014, American Chemical Society. (b) Schematic illustration and optical image of the WSe_2 CMOS structure. The right figure shows its voltage transfer characteristics of the logic inverter with V_{dd} supply from 2 to 6 V [73]. Reproduced with permission from Ref [73]. Copyright 2015, American Chemical Society. (c) Schematic illustration of the graphene field-effect tunneling transistor and the corresponding band structure under operation [74]. Reproduced with permission from Ref [74]. Copyright 2015 American Association for the Advancement of Science (d) Optical image of the graphene/MoS_2/metal vertical transistor device [76]. Reproduced with permission from Ref [76]. Copyright 2013, Nature Publishing Group.

microscope (TEM) images suggest that the atom inter-diffusion (alloy structure) exhibits at the interfaces of these lateral junctions since the TMD alloys are the thermodynamically stable forms. Meanwhile, due to the limitation of the synthetic method, the TMD materials in heterostructures are with one common element either the metal or the chalcogen. Li and co-workers have recently demonstrated a two-step CVD approach for epitaxial growth of WSe_2/MoS_2 lateral junction, where WSe_2 is firstly synthesized through van der Waals epitaxy on substrate followed by the edge epitaxy of MoS_2 along the W growth front (Fig. 4c) [55]. The critical point for the two-step CVD approach is to reveal the reaction condition to avoid the alloy formation during the second-step growth. The TEM image reveals that the atomically sharp interface is obtained at the WSe_2-MoS_2 interface. Similarly, Gong and co-workers also reported a $WSe_2/MoSe_2$ heterojunction by using two-step CVD method [56]. During the second CVD process, WSe_2 bilayer will growth firstly from monolayer $MoSe_2$ edge forming lateral junction and then cover the $MoSe_2$ surface depending on the synthesis time. The two-step growth offers the possibility to construct heterojunctions with varied compositions and desired pattern for scientific research and applications. Besides the novelty of structure, these lateral heterojunction also exhibits intrinsic p–n junction behaviors such as rectifying properties and photovoltaic effects, promising for future monolayer electronics [49,53,55,56].

2D heterostructures and their applications

The recent advances in 2D heterostructures indicate a broad range of applications such as field effect/tunneling transistors, biosensors, light emitting diodes, light detectors, photovoltaic and energy storage devices. The 2D heterostructures and applications reported in the recent five years are summarized in Table 1 and several applications are discussed in the following paragraphs.

Biosensor

The large aspect ratio of 2D materials and their ultrasensitivity to environmental changes make them suitable for possible applications in bio-sensing [10,57]. Previous works have demonstrated the DNA differentiation ability in MoS_2 through its optical and electro-chemical characterization [58,59]. However, MoS_2 is also sensitive with the presence of moisture and oxygen, which limits their applications in aqueous solutions. In order to increase the stability and sensitivity, Loan and co-workers have demonstrated a graphene/MoS_2 heterostructure for label-free selective detection of DNA hybridization through the photoluminescence (PL) intensity changing of MoS_2 (Fig. 5) [60]. The top graphene layer not only avoids the contact of MoS_2 with moisture and oxygen but also hosts the DNA owing to its biocompatibility [60,61]. The detection ability of the graphene/MoS_2 sensor can down to 1 atto mole (10^{-18} M) with few minutes of fast response time, demonstrating the potential of ultrasensitive DNA detection using 2D heterostructures.

Solar cells (photovoltaic)

A solar cell comprises an interface (junction) of two materials with opposite carrier types, which allows efficient carriers separation of the photogenerated electron–hole pairs at the interface to induce the photovoltaic (PV) effect. Although the interface can be easily constructed by forming a Schottky or p–n junction in 2D heterojunctions, the key question is still whether it is possible to achieve enough solar energy conversion within such a thin layer. Bernardi and co-workers have studied the PV effects of 2D heterojunction theoretically, including the Schottky barrier between MoS_2 and graphene and the MoS_2/WS_2 stacking heterostructure [62]. The simulation shows that even the atomically thin active layer can produce power conversion efficiencies (PCE) up to ~1% or a power density of up to 2.5 MW/kg. Compared with the existing ultrathin solar cells, the 2D heterostructure solar cell could achieve 1–3 orders of magnitude higher efficiencies.

Furchi and co-workers have revealed the PV effects on a stacking heterojunction diode made of n-type MoS_2 and p-type WSe_2 monolayers (Fig. 6a) [63]. By adjusting the electrical doping level through a back gate tuning, the 2D hetero-diode shows the PCE about 0.2% and the external quantum efficiency (EQE) about 1.5%. However, the low in-plane mobility of the TMD layer results in a short carrier diffusion time comparable to the interlayer electron–hole recombination lifetime, which leads to the decreased photoresponsivity. In order to overcome the carrier transport issue in this kind of stacking device, Lee and co-workers demonstrate a MoS_2/WSe_2 stacked junction with graphene electrodes directly on the top and the bottom of the heterostructure [64]. The carrier extraction rate is enhanced through the direct charge transfer to graphene semi-metal layer and the photo response has increased about factor of 5. Another similar TMD p–n heterojunction is formed by using p-MoS_2/n-MoS_2 junction. Wi and co-workers demonstrate the PV device with a vertically stacking indium tin oxide (ITO)/n-MoS_2/plasma-doped MoS_2/Au heterostructure (Fig. 6b) [65]. This stacking device exhibits a high short-loop photocurrent density of 20.9 mA/cm^2 (under AM1.5 illumination), PCE of 2.8% and high EQE values from 37 to 78% for the wavelengths between 300 and 700 nm. Tsai and co-workers further utilize CVD MoS_2 monolayers with *p*-Si to form a large scale type II stacking p–n heterojunction, where the built-in electric field near the interface can facilitate photo-generated carrier separation [66]. This large scale heterojunction device can achieve a PCE of 5.23%, and the successful combination of MoS_2 with Si implies the possibility for integrating 2D materials into the Si manufacturing process. Another stacking photovoltaic device is through the formation of simple Schottky barrier with metal(semimetal)/semiconductor junction to establish the built-in electric field at the interface. Shanmugam and co-workers have reported the graphene/WS_2 Schottky barrier solar cell by using WS_2 as a photoactive layer, which shows a good photon absorption ability in the visible spectral range and a photoelectric conversion efficiency about 3.3% [67].

Besides the vertically stacked heterojunction, Gong and co-workers have reported the lateral p–n junction with WS_2/MoS_2 heterostructure, which shows a clear PV effect [49]. An open-loop voltage of 0.12 V and close-loop current of 5.7 pA is measured without further external electrical field tuning. Duan and co-workers forms a lateral heterojunction p–n junction with WSe_2 and WS_2 (Fig. 6c) [53]. The lateral diode shows an open-circuit voltage of ~0.47 V and short-circuit current of ~1.2 nA. The EQE of the photon-to-electron conversion is determined as ~9.9%, and

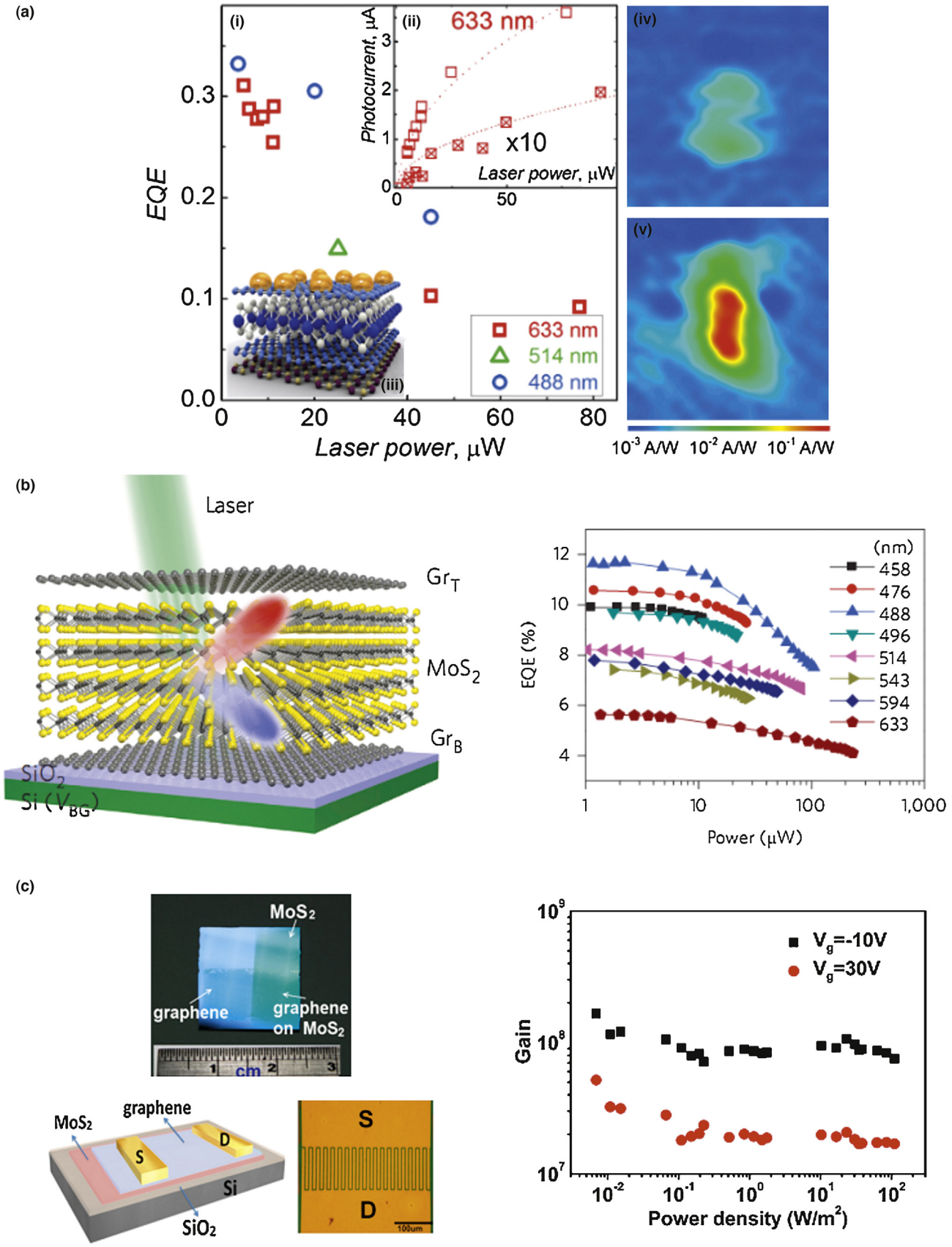

FIGURE 8

Heterostructure for photodetector. (a) External quantum efficiency (EQE) of the graphene/WS_2/graphene heterostructure at different wavelengths and powers. Right image shows the photocurrent maps of h-BN/Gr/MoS_2/Gr devices without (up) and with (down) spattering of gold nanoparticles for plasmonic enhancement [79]. Reproduced with permission from Ref [79]. Copyright 2013, American Association for the Advancement of Science. (b) Schematic illustration of the side view of the graphene/MoS_2/graphene stacking heterostructure device, and the EQE at different laser powers [80].

internal quantum efficiency of ~43%. Li and co-workers further demonstrate a controlled-edge epitaxy lateral WSe_2-MoS_2 monolayer heterojunction. The intrinsic p–n junction exhibits open-circuit voltage of 0.22 V and close-circuit current of 7.7 pA under white light illustration, and a PCE at least 0.2% [55]. The smaller photo active area and the monolayered thickness in these in-plane solar cells might restrict their solar absorption. The low PCE issue may be resolved by introducing metallic nanoparticles or photonic structures on it.

Field effect transistors

Although graphene shows potential in realizing 2D high speed bipolar field effect transistor (FET) devices due to its high carrier mobility and ambipolar effect, the zero band gap and Klein tunneling nature limit its application for FET due to low ON/OFF current ratios. One approach for realizing high performance 2D FETs is to use TMD as the channel material. The proper bandgap and reasonable mobility of the TMD materials make them more promising than graphene. Roy and co-workers have demonstrated an n-type MoS_2 FET with all components formed by 2D materials, including MoS_2 as the active channel material, h-BN as the dielectric layer for top electrode isolation, and graphene as the semi-metal contacts (Fig. 7a) [68]. The high mobility and tunable Fermi-level properties of graphene allow it to from an Ohmic contact with TMD materials. The h-BN layers can act as an isolating layer with its large bandgap, and it has atomically smooth surfaces without charge trapping, making it a great interface or substrate for 2D materials [42]. The MoS_2 n-type FET exhibits an ON/OFF ratio larger than 10^6, and an electron mobility of ~33 cm^2/V s. Likewise, a p-type FET has been demonstrated using WSe_2 as the active channel [13]. Since WSe_2 is a slightly p-doped material, it is easy to tune the transport carrier types by extra doping or by selection of the contact metal to serve for n-type or p-type FETs [13,69,70]. Furthermore, the complementary metal oxide semiconductor (CMOS) has been reported by using two different channel materials [71] or materials with different doping levels [70,72,73]. Yu and co-workers have demonstrated the high performance CMOS by using WSe_2 as the main active channel and tune the carrier channel through chemical doping (Fig. 7b) [73]. This WSe_2 CMOS exhibits full logic swing, ideal voltage transfer characteristic, high noise margin and large voltage gain up to 38 in inverter operation, promising for low power electronic devices.

Vertical transport through 2D heterojunctions is another type of 2D FET. Britnell and co-workers have reported a tunneling FET with the vertically stacked heterostructure composed of graphene and thin h-BN or MoS_2 (Fig. 7c) [74]. The basic principle is based on the quantum tunneling, where the graphene electrodes are separated by thin insolation barriers (h-BN or MoS_2) and the tunneling is controlled by tuning the density of states in graphene and adjoined barrier by an external voltage. The tunneling FET exhibits an ON/OFF ratio of ~50 and ~10^4 by using BN and MoS_2 as barrier, respectively. The transit time is expected to be much faster than planar FET by tunneling mechanism, which is potential for high-speed operation. Sharing the same idea, Georgiou and co-workers have reported a graphene vertical FET by using WS_2 layers as barrier. The small band gap of WS_2 not only allows for tunneling transport but also for thermionic transport by electrically tuning the Fermi-level of graphene. Meanwhile, it exhibits a high ON current and better current modulation with an ON/OFF current ratio up to 10^6 [75]. This device can further operate stably on transparent and flexible substrates with similar performance on SiO_2 substrates. Another type of vertical FET is simply with the structure of graphene/TMD/metal, where proper metal layer provides an Ohmic contact with TMD to facility carrier transport and the current modulation is completed by electrical tuning through Schottky barrier between graphene and TMD layers. Yu and co-workers have reported a vertical FET with a graphene/few-layer MoS_2/metal heterostructure, which exhibits an ON/OFF ratio larger than 10^3 and high current density of 5000 A/cm^2 (Fig. 7d) [76]. Moriya and co-workers further improved the current modulation to larger than 10^5 and current density up to 10^4 A/cm^2 with a similar structure but better interface fabrication [77]. The advantages of this type of vertical FETs are the large current density and the small device scale, providing high potential for future high-density integration circuits. Besides the above commercial tunneling FETs, Sarkar and co-workers have recently revealed a band-to-band tunnel FET with the vertical stacking heterojunction of p-type Ge and n-type MoS_2, where its subthreshold swing (SS) 31.1 mV/decades is significantly lower than the thermionic limitation [78]. Their results open a venue for future high-performance and low power electronics.

Photodetector

The zero band gap and high mobility properties of graphene can provide broadband absorption and fast response time in photoelectronics, but the zero gap nature and weak optical absorption limit the photoresponsivity. The monolayer TMD materials have a direct band gap and thus a high absorption coefficient. However, the low mobility of TMDs will reduce the response time and extraction rate. Therefore, the development in related heterostructures is trying to combine both advantages to enhance the photoresponses. Britnell and co-workers have demonstrated an efficient photodetector with graphene/TMDs/graphene stacking heterostructures (Fig. 8a) [79]. The TMDs layers serve as a light absorber and the graphene electrodes can provide good carrier separation by tuning its Fermi level through doping. The combined heterostructure (graphene/WS_2/graphene) for PV devices shows photoresponsivity above 0.1 A/W, corresponding to the EQE up to 30%. Furthermore, Yu and co-workers provide an extra gate voltage control in graphene/MoS_2/graphene heterostructure to adjust the schottky barrier between graphene and MoS_2, where the external electrical field can enhance the photo-carrier generation, separation and transport processes in this vertical stacking device (Fig. 8b) [80]. It has been demonstrated that the EQE can achieve 55% and 85% of internal quantum efficiency (IQE) by proper photocurrent modulation. Lee and co-workers have extended the range of these vertical stacking heterostructure through inducing p–n junction into the

Reproduced with permission from Ref [80]. Copyright 2013, Nature Publishing Group. (c) Schematic illustration and optical image of the large-area graphene/MoS_2 stacking photodetector, and the photogain at different laser powers [89]. Reproduced with permission from Ref [89]. Copyright 2014, Nature Publishing Group.

photovoltaic device, where the MoS_2/WSe_2 p–n junction is sandwiched by graphene electrodes [64]. The p–n junction can facilitate photo-excited electron–hole separation and the EQE has been shown to be dependent on the thickness of p–n junction. Cheng and co-workers have fabricated a vertical p–n junction by monolayer CVD WSe_2 and multilayer exfoliated MoS_2 [81]. The device shows photoresponses on entire overlapping area with a maximum EQE up to 12%. Similarly, Deng and co-workers report a p–n diode based on a p-type black phosphorus/n-type monolayer MoS_2 stacked p–n heterojunction [82]. The black phosphorus is an intrinsic p-type semiconductor with a high carrier mobility value (~10,000 cm^2/Vs) and a small direct band gap about 0.3 eV in monolayer, suitable for broadband photodetectors. This black phosphorus/MoS_2 heterojunction exhibits the photo-responsivity of 418 mA/W and EQE of 0.3% under 633 nm laser illumination, potentially useful for broadband photodetectors. It is noteworthy that the electroluminescence peaks have been observed at various junctions including vertically stacked p–n junction [81,83], electrical field induced junction [84–87], and double heterojunction [88], suggesting the possibility of using TMD for LED devices.

Besides above mentioned heterostructures, the simple graphene/TMD heterojunction can provide sensitive photodetection by properly tuning the electrical potential at the interface. Zhang and co-workers have constructed a large area graphene/MoS_2 heterojunction with monolayer CVD graphene and MoS_2, where the electrodes are contacted only on top graphene layer and the MoS_2 is covered by graphene (Fig. 8c) [89]. The photo-excited electrons from MoS_2 will transport to graphene and the holes are trapped in MoS_2 based on the tunable build-in potential at the interface. At the same time, the high mobility in graphene will facilitate the electron extraction, but the holes will be trapped in MoS_2 resulting in a multiple recirculation of electrons in graphene. The recirculation phenomenon leads to a photogain higher than 10^8 and a photoresponsivity larger than 10^7 A/W. On the other hand, Roy and co-workers shows that the graphene/multi-layer MoS_2 heterojunction not only provides a high photoresponsivity near 5×10^8 A/W but also exhibits persistent photoconductivity through electric field tuning, which can serve as gate-tunable photodetectors and optical switches [90].

Thermoelectric devices

On the basis of the layered stacking structure, the heat dissipation in 2D herterostructures is limited by the thermal transport in vertical direction [91]. The temperature gradient can be easily built in few-layer 2D materials or vertical heterostructures, potential for applications in thermoelectrics. Chen and co-workers have reported a Seebeck study on a graphene/h-BN/graphene heterostructure [92]. Through applying a temperature gradient on top and bottom graphene layers and measuring the thermoelectric voltage, the heterostructure shows a Seebeck coefficient about −99 μV/K. Together with the electrical and thermal conductance, the power factor (S^2G) of 1.51×10^{-15} W/K^2 and the thermoelectric figure of merit $ZT = 1.05 \times 10^{-6}$ can be derived. Although the thermoelectric energy conversion efficiency is still low in this device, the research area is at an early stage and it is anticipated that progresses can be made in the near future.

Conclusion

We summarize the recent progresses on the fabrication and applications of 2D vertical and lateral heterostructures in this review. The various heterostructures based on 2D materials open a new research field and the band structure engineering by heterostructure formation provides the possibility to develop novel devices with desired properties and potential energy applications. It is anticipated that the further progresses in 2D material growth, heterostructure formation and device fabrication shall lead to practical applications in the future.

Acknowledgements

L.J.L. thanks support from KAUST Saudi Arabia, Academia Sinica Taiwan and AOARD-134137 USA.

References

[1] Z.I. Alferov, Rev. Mod. Phys. 73 (3) (2001) 767.
[2] H. Kroemer, Rev. Mod. Phys. 73 (3) (2001) 783.
[3] A. Isamu, et al. J. Lumin. 48–49 Part 2 (1991) 666.
[4] H. Amano, et al. Jpn. J. Appl. Phys. 28 (12A) (1989) L2112.
[5] K.K. Kim, et al. Nano Lett. 12 (1) (2011) 161.
[6] Y. Shi, et al. Nano Lett. 10 (10) (2010) 4134.
[7] C.-H. Chen, et al. 2D Mater. 1 (3) (2014) 034001.
[8] K.-K. Liu, et al. Nano Lett. 12 (3) (2012) 1538.
[9] X. Li, et al. Science 324 (5932) (2009) 1312.
[10] C.-H. Chen, et al. Small 8 (1) (2012) 43.
[11] RadisavljevicB, et al. Nat. Nanotechnol. 6 (3) (2011) 147.
[12] Q. He, et al. Small 8 (19) (2012) 2994.
[13] H. Fang, et al. Nano Lett. 12 (7) (2012) 3788.
[14] J.-K. Huang, et al. ACS Nano 8 (1) (2013) 923.
[15] J. Pu, et al. Nano Lett. 12 (8) (2012) 4013.
[16] A.K. Geim, I.V. Grigorieva, Nature 499 (7459) (2013) 419.
[17] H. Wang, et al. Nanoscale 6 (21) (2014) 12250.
[18] M. Buscema, et al. Chem. Soc. Rev. 44 (11) (2015) 3691.
[19] K.S. Novoselov, et al. Science 306 (5696) (2004) 666.
[20] S. Kar, S. Talapatra, in: B. Bhushan (Ed.), Encyclopedia of Nanotechnology, Springer, Netherlands, 2012, p. 2630.
[21] C.-Y. Su, et al. ACS Nano 5 (3) (2011) 2332.
[22] B. Lung-Hao Hu, et al. Nat. Commun. 4 (2013) 1687.
[23] J.N. Coleman, et al. Science 331 (6017) (2011) 568.
[24] E. Benavente, et al. Coord. Chem. Rev. 224 (1–2) (2002) 87.
[25] A.S. Golub, et al. Russ. Chem. Rev. 72 (2) (2003) 123.
[26] M.A. Lukowski, et al. J. Am. Chem. Soc. 135 (28) (2013) 10274.
[27] Z. Zeng, et al. Angew. Chem. Int. Ed. 50 (47) (2011) 11093.
[28] Z. Zeng, et al. Angew. Chem. Int. Ed. 51 (36) (2012) 9052.
[29] X. Li, et al. J. Am. Chem. Soc. 133 (9) (2011) 2816.
[30] A.M. van der Zande, et al. Nat. Mater. 12 (6) (2013) 554.
[31] S. Najmaei, et al. Nat. Mater. 12 (8) (2013) 754.
[32] Y.-H. Lee, et al. Adv. Mater. 24 (17) (2012) 2320.
[33] Y. Zhang, et al. ACS Nano 7 (10) (2013) 8963.
[34] H.R. Gutiérrez, et al. Nano Lett. 13 (8) (2012) 3447.
[35] X. Lu, et al. Nano Lett. 14 (5) (2014) 2419.
[36] Y.-H. Chang, et al. ACS Nano 8 (8) (2014) 8582.
[37] Y.-C. Lin, et al. Nanoscale 4 (20) (2012) 6637.
[38] D. Kong, et al. Nano Lett. 13 (3) (2013) 1341.
[39] R. Morrish, et al. Chem. Mater. 26 (13) (2014) 3986.
[40] A.L. Elías, et al. ACS Nano 7 (6) (2013) 5235.
[41] K.S. Kim, et al. Nature 457 (7230) (2009) 706.
[42] C.R. Dean, et al. Nat. Nanotechnol. 5 (10) (2010) 722.
[43] W.-T. Hsu, et al. ACS Nano 8 (3) (2014) 2951.
[44] H. Fang, et al. Proc. Natl. Acad. Sci. U. S. A. 111 (17) (2014) 6198.
[45] M.-H. Chiu, et al. ACS Nano 8 (9) (2014) 9649.
[46] W. Yang, et al. Nat. Mater. 12 (9) (2013) 792.
[47] Y. Shi, et al. Nano Lett. 12 (6) (2012) 2784.
[48] Y.-C. Lin, et al. ACS Nano 8 (4) (2014) 3715.
[49] Y. Gong, et al. Nat. Mater. 13 (2014) 1135.
[50] Y.-C. Lin, et al. Nat. Commun. 6 (2015) 7311.
[51] M.P. Levendorf, et al. Nature 488 (7413) (2012) 627.

[52] J. Lu, et al. Nano Lett. 14 (9) (2014) 5133.
[53] X. Duan, et al. Nat. Nanotechnol. 9 (2014) 1024.
[54] C. Huang, et al. Nat. Mater. 13 (2014) 1096.
[55] M.-Y. Li, et al. Science 349 (6247) (2015) 524.
[56] Y. Gong, et al. Nano Lett. 15 (9) (2015) 6135.
[57] C.-H. Chen, et al. Nanomed. Nanotechnol. Biol. Med. 9 (5) (2013) 600.
[58] C. Zhu, et al. J. Am. Chem. Soc. 135 (16) (2013) 5998.
[59] A.H. Loo, et al. Nanoscale 6 (20) (2014) 11971.
[60] P.T.K. Loan, et al. Adv. Mater. 26 (28) (2014) 4838.
[61] K.F. Mak, et al. Nat. Mater. 12 (3) (2013) 207.
[62] M. Bernardi, et al. Nano Lett. 13 (8) (2013) 3664.
[63] M.M. Furchi, et al. Nano Lett. 14 (8) (2014) 4785.
[64] C.-H. Lee, et al. Nat. Nanotechnol. 9 (9) (2014) 676.
[65] S. Wi, et al. ACS Nano 8 (5) (2014) 5270.
[66] M.-L. Tsai, et al. ACS Nano 8 (8) (2014) 8317.
[67] M. Shanmugam, et al. Nanoscale 6 (21) (2014) 12682.
[68] T. Roy, et al. ACS Nano 8 (6) (2014) 6259.
[69] H. Fang, et al. Nano Lett. 13 (5) (2013) 1991.
[70] M. Tosun, et al. ACS Nano 8 (5) (2014) 4948.
[71] H. Liu, et al. ACS Nano 8 (4) (2014) 4033.
[72] S. Das, A. Roelofs, 2014 72nd Annual Device Research Conference (DRC), 2014, . p. 185.
[73] L. Yu, et al. Nano Lett. 15 (8) (2015) 4928.
[74] L. Britnell, et al. Science 335 (6071) (2012) 947.
[75] T. Georgiou, et al. Nat. Nanotechnol. 8 (2) (2013) 100.
[76] W.J. Yu, et al. Nat. Mater. 12 (3) (2013) 246.
[77] R. Moriya, et al. Appl. Phys. Lett. 105 (8) (2014) 083119.
[78] D. Sarkar, et al. Nature 526 (7571) (2015) 91.
[79] L. Britnell, et al. Science 340 (6138) (2013) 1311.
[80] W.J. Yu, et al. Nat. Nanotechnol. 8 (12) (2013) 952.
[81] R. Cheng, et al. Nano Lett. 14 (10) (2014) 5590.
[82] Y. Deng, et al. ACS Nano 8 (8) (2014) 8292.
[83] O. Lopez-Sanchez, et al. ACS Nano 8 (3) (2014) 3042.
[84] A. Pospischil, et al. Nat. Nano 9 (4) (2014) 257.
[85] B.W.H. Baugher, et al. Nat. Nano 9 (4) (2014) 262.
[86] J.S. Ross, et al. Nat. Nano 9 (4) (2014) 268.
[87] Y.-J. Zhang, et al. Science 344 (6185) (2014) 725.
[88] F. Withers, et al. Nat. Mater. 14 (3) (2015) 301.
[89] W. Zhang, et al. Sci. Rep. 4 (2014) 3826.
[90] K. Roy, et al. Nat. Nanotechnol. 8 (11) (2013) 826.
[91] E. Pop, et al. MRS Bull. 37 (12) (2012) 1273.
[92] C.-C. Chen, et al. Nano Res. 8 (2) (2015) 666.
[93] X. Hong, et al. Nat. Nanotechnol. 9 (9) (2014) 682.
[94] G.-H. Lee, et al. ACS Nano 7 (9) (2013) 7931.